THE JOURNAL OF PHYSICAL CHEMISTRY B
A JOURNAL OF THE AMERICAN CHEMICAL SOCIETY

pubs.acs.org/JPCB

Article

Diketopiperazine Formation from FPG$_n$K (n = 1−9) Peptides: Rates of Structural Rearrangements and Mechanisms

Zhichao Zhang, Christopher R. Conant, Tarick J. El-Baba, Shannon A. Raab, Daniel R. Fuller, David A. Hales,* and David E. Clemmer*

Cite This: *J. Phys. Chem. B* 2021, 125, 8107−8116

Read Online

ACCESS | Metrics & More | Article Recommendations | Supporting Information

ABSTRACT: Peptides with penultimate proline residues undergo *trans* → *cis* isomerization of the Phe^1−Pro^2 peptide bond followed by spontaneous bond cleavage at the Pro^2−Xxx^3 bond (where Xxx is another amino acid residue), leading to cleavage of the Pro^2−Xxx^3 bond and formation of a diketopiperazine (DKP). In this paper, ion mobility spectrometry and mass spectrometry techniques were used to study the dissociation kinetics of nine peptides [Phe^1−Pro^2−Gly$_n$−Lys^{n+3} (n = 1−9)] in ethanol. Shorter (n = 1−3) peptides are found to be more stable than longer (n = 4−9) peptides. Alanine substitution studies indicate that, when experiments are initiated, the Phe^1−Pro^2 bond of the n = 9 peptide exists exclusively in the *cis* configuration, while the n = 1−8 peptides appear to exist initially with both *cis*- and *trans*-Phe^1−Pro^2 configured bonds. Molecular dynamics simulations indicate that intramolecular hydrogen bonding interactions stabilize conformations of shorter peptides, thus inhibiting DKP formation. Similar stabilizing interactions appear less frequently in longer peptides. In addition, in smaller peptides, the N-terminal amino group is more likely to be charged compared to the same group in longer peptides, which would inhibit the dissociation through the DKP formation mechanism. Analysis of temperature-dependent kinetics measurements provides insight about the mechanism of bond cleavage. The analysis gives the following transition state thermochemistry: $\Delta G^{\ddagger}$ values range from 94.6 ± 0.9 to 101.5 ± 1.9 kJ·mol^{-1}, values of $\Delta H^{\ddagger}$ range from 89.1 ± 0.9 to 116.7 ± 1.5 kJ·mol^{-1}, and $\Delta S^{\ddagger}$ values range from −25.4 ± 2.6 to 50.8 ± 4.2 J·mol^{-1}·K^{-1}. Proposed mechanisms and thermochemistry are discussed.

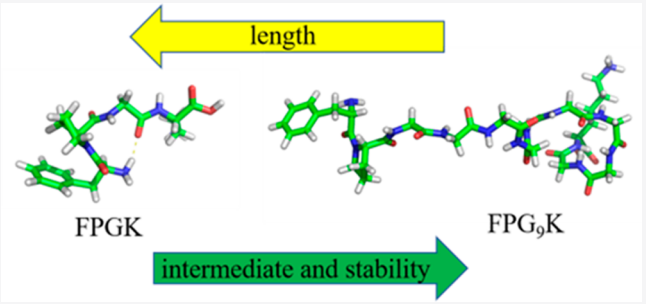

INTRODUCTION

While detailed structural information is widely available for proteins,[1−5] the conformations, stabilities, and structural transitions of smaller peptides have been largely ignored.[6] The stability of these smaller amino acid chains is especially important, as many are biologically active and some are relevant to the design of peptide therapeutics.[7−10] Several potential degradation pathways may occur during the storage of peptides and proteins, including hydrolysis,[11] deamidation,[11,12] oxidation,[13] racemization,[12,14] and bond cleavage, resulting in formation of a diketopiperazine (DKP).[15] DKP formation is common among peptides containing a penultimate proline, and many such peptides are biologically active.[16] In this degradation pathway, the first two amino acids cyclize upon nucleophilic attack of the N-terminal amine to the electrophilic carbonyl carbon between the second and third amino acid residues,[17] resulting in bond cleavage and the formation of DKP and a new shorter amino acid peptide chain, as shown in Scheme 1.

Understanding the factors that influence DKP formation is relevant for potential immunotherapies in development. For example, peptides having penultimate prolines have received substantial attention as a means of suppressing various

Scheme 1. Cleavage Mechanism of Pro2−Gly3 by DKP Formation with Phe1−Pro2 in the *cis*-Configuration (n = 1−9)

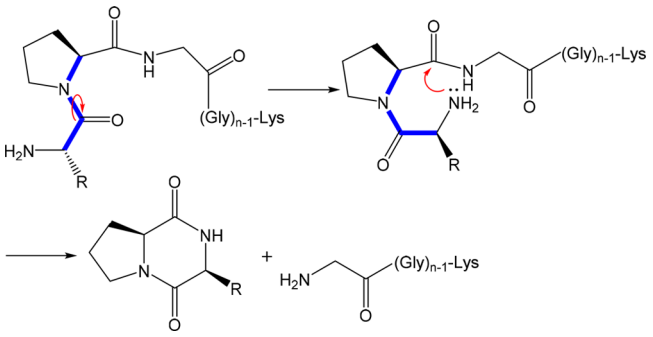

Received: April 20, 2021
Revised: June 30, 2021
Published: July 16, 2021

https://doi.org/10.1021/acs.jpcb.1c03515
J. Phys. Chem. B 2021, 125, 8107−8116

cancers.[18,19] Peptides binding to the major histocompatibility complex are known to be involved with cellular recognition by the immune system.[20,21] One promising therapeutic application is to utilize peptides found exclusively in cancerous cells as vaccines.[22] Since penultimate proline favors degradation through DKP formation,[15] for these peptide-based potential cancer targets to be effective, the stability of these peptides, especially as it pertains to degradation by DKP formation, should be considered.[23,24]

Here, we use ion mobility spectrometry (IMS) combined with MS to systematically study how peptide length affects DKP formation rates, extending our earlier studies of how proline influences peptide conformations.[25−27] Different conformations are separated by IMS based on differences in collision cross sections (CCS),[28,29] allowing *trans*- and *cis*-isomers involved in the DKP formation process to be resolved. Previous studies, such as the dissociation of bradykinin (Arg^1−Pro^2−Pro^3−Gly^4−Phe^5−Ser^6−Pro^7−Phe^8−Arg^9), provide evidence for a slow protonation event mediated by a structural change.[25] A study of the peptide substance P (Arg^1−Pro^2−Lys^3−Pro^4−Gln^5−Gln^6−Phe^7−Phe^8−Gly^9−Leu^{10}−Met^{11}), involved in inflammation, pain, and control of blood pressure,[30−34] presents two sequential bond cleavage events.[27] Additionally, we find that DKP formation rates depend strongly on the environment (in particular, the properties of the solvent),[35] suggesting that, in addition to enzymatic processes,[36] peptide stability will depend upon where the peptide resides within the cell. Below, we explore how amino acid chain length influences degradation kinetics in solutions of ethanol. Although DKP dissociation kinetics have been reported before,[37−40] these studies are primarily limited to dipeptide and tripeptide esters and amides. This represents the first systematic study focusing on how peptide length influences stability. Here, we monitor the dissociation of a peptide having different lengths of a polyglycine linker [Phe^1−Pro^2−Gly_n−Lys^{n+3} (n = 1−9)] with IMS-MS to investigate the influence on dissociation kinetics (i.e., DKP formation). The rates of configurational changes of proline residues are known to depend strongly on solvent; more polar solvents favor *cis*-configurations, whereas relatively nonpolar solvents favor *trans*-proline bonds.[41−43] While we have shown that these configurational changes occur in a range of alcohols (propanol, ethanol, methanol) and water,[35] the experiments described below are carried out in ethanol because the rates of configurational changes as well as DKP formation lie in an intermediate range that is straightforward to measure. The results reported below show that variations in conformation due to length influence peptide stability. Detailed mechanisms and thermochemistry are discussed.

EXPERIMENTAL SECTION

Peptide Synthesis. All peptides that are analyzed in this paper were synthesized using 0.1 mmol of Fmoc protected amino acids and Lys-Rink-residue [purchased from Midwest Biotech (Indianapolis, IN)] using an ABI 433A peptide synthesizer according to a standard solid state peptide synthesis protocol.[44] Briefly, 6-Cl-HOBt (hydroxybenzotriazole) and *N*,*N*′-diisopropylcarbodiimide were used as coupling reagents. Cleavage was performed by treating the product with 10 mL of trifluoroacetic acid (TFA) solution containing 2.5% triisopropylsilane and 2.5% H_2O at room temperature for 1.5 h. The resulting product was filtered, and the peptide was precipitated and washed three times with cold ether (10 mL each time). The purified peptide was lyophilized, yielding the product as a white, fluffy solid.

Sample Preparation and Electrospray Ionization (ESI) Conditions. Detailed descriptions of sample preparation, ESI conditions, and the protocol used for kinetics studies can be found elsewhere.[25,27,45] Briefly, 500 μM stock solutions of Phe^1−Pro^2−Gly_n−Lys^{n+3} (n = 1−9) were prepared in pure ethanol and then stored at −20 °C. These samples were diluted to 20 μM in ethanol with 1% acetic acid (by volume) before loading onto a Nano-ESI (Triversa nanomate, Advion Biosciences, Ithica, NY) auto sampler used to initiate the spray. The ESI voltage was maintained at 1.2 kV for all measurements.

IMS-MS Instrumentation and Kinetics Measurements. During the kinetics measurements, each sample was incubated independently in a water bath at a defined temperature, and IMS-MS measurements were made at defined time intervals. Each kinetics experiment was carried out in triplicate using different samples of each peptide. Structural transitions and decomposition processes were monitored on a home-built 2 m drift tube instrument coupled with a time-of-flight (TOF) mass analyzer (see the Supporting Information, Figure S1). Detailed descriptions are provided elsewhere.[29,46−53] Briefly, ions produced by ESI are transmitted from ambient (room) pressure through a capillary, accumulated in an ion funnel,[54] and with ∼150 μs electrostatic gate pulses are periodically introduced into the drift tube. The drift tube is filled with ∼3 Torr (4 mbar) of 298 K He buffer gas. Ions separate as they travel through the buffer gas under the influence of a weak uniform electric field (∼10 $V{\cdot}cm^{-1}$) based on differences in their mobilities through the gas. As the ions exit the drift tube, they are pulsed into an orthogonal TOF mass spectrometer and detected.[55] In many cases, it is helpful to convert the measured drift time (t_D) distribution scale into a CCS (Ω) scale, because this reflects the rotationally average size of different conformations. This is done using the equation[48]

$$\Omega = \frac{(18\pi)^{1/2}}{16}\frac{ze}{(k_bT)^{1/2}}\left[\frac{1}{m_I}+\frac{1}{m_B}\right]^{1/2}\frac{t_DE}{L}\frac{760}{P}\frac{T}{273.2}\frac{1}{N} \quad (1)$$

where the relevant terms are ion charge (ze), Boltzmann's constant (k_b), mass of the ion (m_I), mass of the buffer gas (m_B), temperature (T), electric field value (E), drift tube length (L), pressure of buffer gas (P), and buffer gas neutral number density (N).

Molecular Dynamics (MD) Simulations. In order to understand the types of conformations that might be favored in solution, we have also carried out a series of MD simulations. These simulations were performed using the Gromacs 2018.3 suite of software (available at https://www.gromacs.org/Downloads).[56] Instead of using the doubly charged precursor ion as captured with IMS-MS, singly charged peptides are selected for the simulation because of the following reasons: (1) The DKP formation reaction will not occur when there is a protonated amino group on the N-terminus; therefore, these peptides exist in solution with a neutral amino group on Phe^1. (2) The peptides are incubated in ethanol with 1% acetic acid; thus, the carboxylic group and side chain of Lys^7 are likely to be protonated. Phe^1−Pro^2−Gly_n−Lys^{n+3} (n = 1, 2, and 9) was selected to gain an insight into why shorter peptides are more stable than longer peptides in this family. The simulations started with the *cis*- and *trans*-isomers of the n = 1 and 2

https://doi.org/10.1021/acs.jpcb.1c03515
J. Phys. Chem. B 2021, 125, 8107−8116

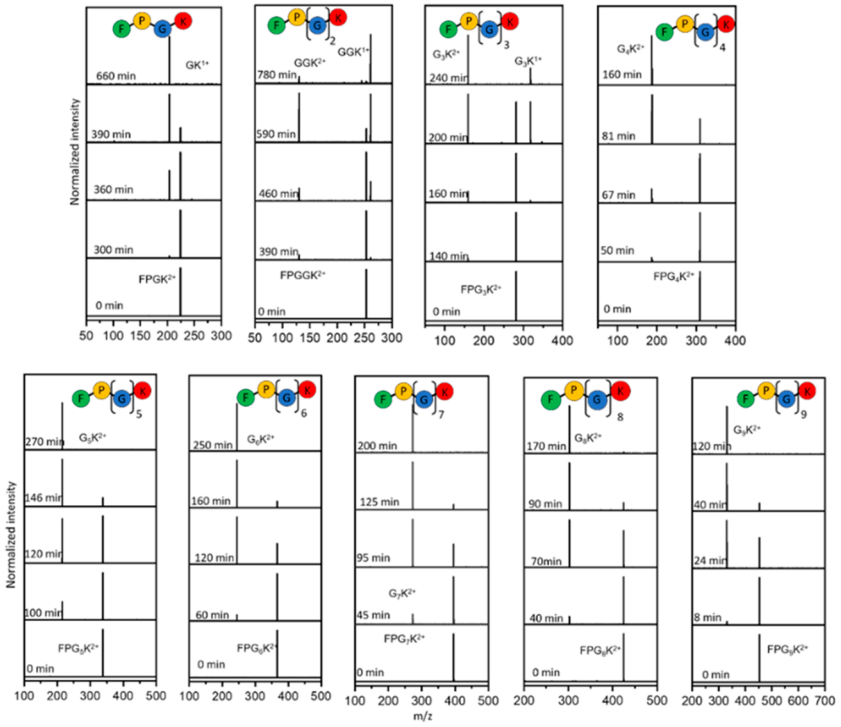

Figure 1. Peptide Phe[1]−Pro[2]−Gly$_n$−Lys^{n+3} (n = 1−9) dissociation mass spectra in ethanol at 75 °C with 1% acetic acid (by volume). Self-cleavage of the Pro[2]−Gly[3] bond occurs during the incubation.

peptides and the *cis*-conformer of the n = 9 peptide. In every case, the singly charged ions with protonation on the side chain of C-terminus lysine are used. Our simulations are based on calculations that utilize a *leapfrog integrator* having a 2 fs time step. The atomic coordinates of the structures that are used in the simulations were generated with PyMOL 1.6 software.[57] Charges on basic sites were set with the *gmx pdb2gmx* command. While all of the experiments that are reported here are carried out in ethanol, all of the simulations use force fields that were developed for water. We note that experiments performed on Phe[1]−Pro[2]−Gly$_8$−Lys[11] in water, methanol, ethanol, and propanol (as well as other studies of different solvents) indicate that, although the abundances of different structures vary with solvent, peaks in the cross section distributions indicate that the conformations are the same (i.e., the resulting ions have CCSs that are identical within the experimental uncertainties). Simulations are acquired for 1 ns using the optimized potential for liquid simulations (OPLS-AA) force field for water.[58] In this approach, a simple point-charge water model[59] in a cubic box with periodic boundary conditions is used. A minimum distance of 1 nm between the peptide and the boundaries of the box was applied. The short-range cutoff for electrostatic and van der Waals was set to 1.0 nm. Beyond 1 nm, the program used the particle mesh Ewald method for electrostatic interactions to simulate long-range interactions.[60] Single negatively charged chloride ions were added to the peptide solution to neutralize charges. The simulations were performed at 300 K.

RESULTS AND DISCUSSION

Mass Spectral Data for [FPG$_n$K + 2H]$^{2+}$ Dissociation. The precursor peptides in this study form exclusively doubly charged [FPG$_n$K + 2H]$^{2+}$ ions under our ESI conditions. Dissociation of precursor peptide by DKP formation leaves a G$_n$K peptide fragment. The G$_n$K dissociation product forms only doubly protonated [G$_n$K + 2H]$^{2+}$ ions for the heavier peptides in this study (n > 3). For peptides containing n = 2−3, both the singly and doubly charged product ions [G$_n$K + H]$^+$ and [G$_n$K + 2H]$^{2+}$ are produced. Only the singly charged product ion is observed for the case of n = 1. However, in every case, we are able to follow the precursor and total product signals over time. Representative mass spectra recorded by IMS-MS for dissociation of Phe[1]−Pro[2]−Gly$_n$−Lys^{n+3} (n = 1−9) in ethanol at 75 °C are shown in Figure 1. These demonstrate the gradual shift over time from precursor to product ions.

Table 1 and Figure 2 show dissociation half-lives as a function of glycine linker length. It is obvious that the rate of DKP formation generally increases with the number of glycine residues. Phe[1]−Pro[2]−Gly$_2$−Lys[5] is the most stable peptide in

Table 1. Dissociation Half-Lives

	dissociation half-life[b] (min)		
n[a]	75 °C	70 °C	65 °C
1	369 ± 5	561 ± 11	1174 ± 37
2	487 ± 5	856 ± 7	1537 ± 22
3	166 ± 1	303 ± 5	462 ± 18
4	74 ± 3	132 ± 6	192 ± 7
5	115 ± 2	187 ± 4	322 ± 8
6	101 ± 1	137 ± 2	236 ± 10
7	78 ± 1	152 ± 2	242 ± 7
8	70 ± 6	102 ± 6	165 ± 8
9	25 ± 1	42 ± 1	79 ± 2

[a]n corresponds to the number of glycine residues. [b]The reported dissociation half-lives are the averaged value and standard deviation from triplicate measurements.

https://doi.org/10.1021/acs.jpcb.1c03515
J. Phys. Chem. B 2021, 125, 8107−8116

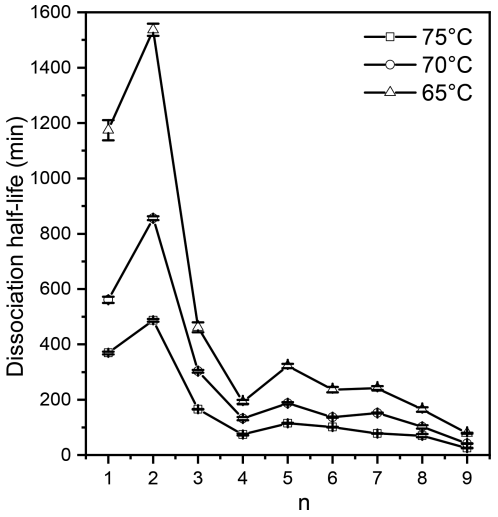

Figure 2. Dissociation half-life of peptides with different lengths of polyglycine linkers under 75 °C (hollow rectangles), 70 °C (circles), and 65 °C (hollow triangles) in ethanol with 1% acetic acid (by volume). *n* is the length of polyglycine linker. Shorter peptides are more stable than longer ones.

this family, while peptide Phe[1]–Pro[2]–Gly_9–Lys^{12} is the least stable one.

Determination of Penultimate Proline Configuration. To assign the penultimate prolines' configuration in these peptides, we performed alanine substitution experiments (Pro[2]–Ala). Where Pro allows both *trans*- and *cis*-isomers, Ala is exclusively *trans*. Therefore, if the structure does not change after alanine substitution, we will assign the proline as the *trans* configuration; otherwise, we will assign the proline as the *cis* configuration. Figure 3 shows the collision cross section distribution of doubly charged peptide Phe[1]–Pro[2]–Gly_n–Lys^{n+3} (n = 3, 5, and 9) and their alanine substituted analogues Phe[1]–Ala[2]–Gly_n–Lys^{n+3} (n = 3, 5, and 9) acquired using IMS-MS (analogous data for other peptides are shown in Supporting Information Figure S2). The CCS values for the

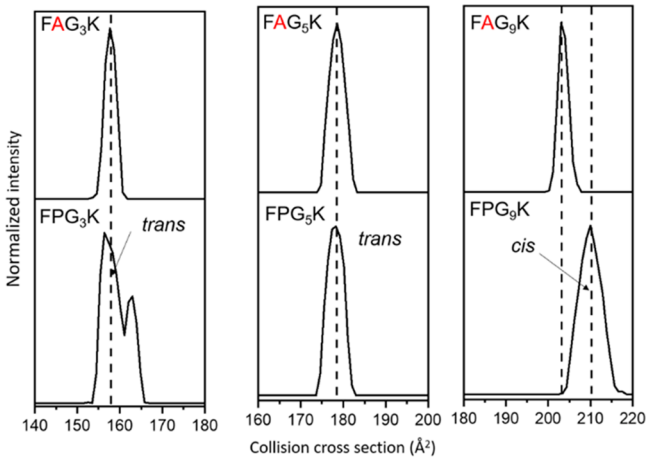

Figure 3. Collison cross section distribution for n = 3, 5, and 9 peptides with their Pro[2] to Ala substituted peptides. Distributions are acquired in ethanol with 1% acetic acid (by volume). Alanine substituted peptides are shown on top of the corresponding non-substituted peptides. Distributions for Ala substituted peptides are corrected with intrinsic size parameter between Pro and Ala residues. Ala-substituted peptides are corrected based on the amino acid intrinsic size parameter as described previously.[61]

The IMS distribution for the Phe[1]–Pro[2]–Gly_9–Lys^{12} peptide is the only measurement that shows no peak at the same CCS as found for the peptide containing the Pro[2]–Ala substitution. We interpret this result to imply that the Phe[1]–Pro[2]–Gly_9–Lys^{12} peptide contains a *cis*-Pro[2] bond. This finding is consistent with the dissociation rate for this peptide, which is the fastest among all of the peptides studied here. Each of the Phe[1]–Pro[2]–Gly_n–Lys^{n+3} (n = 1, 2, 4, 5, 6, and 7) peptides shows a single peak in the CCS distribution profile. These peaks align with their Pro[2]–Ala substituted peptides. We interpret this as an indication that the Phe[1]–Pro[2]–Gly_n–Lys^{n+3} (n = 1, 2, 4, 5, 6, and 7) peptides each contain a *trans*-Pro[2] bond. In our previous study, Phe[1]–Pro[2]–Gly_8–Lys^{11} shows two mobility peaks corresponding to *cis*- and *trans*-configured proline isomers.[35] Phe[1]–Pro[2]–Gly_3–Lys^6 shows obvious multiple conformations with two peaks at Ω = 156 ± 2 Å[2] and Ω = 162 ± 3 Å[2]. The alanine substituted peptide peaks at Ω = 157 ± 3 Å[2]. This suggests Phe[1]–Pro[2]–Gly_3–Lys^6 includes a conformer with *trans*-configured proline at ~157 ± 3 Å[2], while the other conformations contain *cis*-configured proline.

CCS Distributions of Precursor Ions during Dissociation. The $^{DT}CCS_{He}$ distributions of $[FPG_3K + 2H]^{2+}$ have multiple features at 156, 158, and 162 Å[2], indicating that multiple backbone conformations may be present (Figure 3). We modeled the IMS distributions using a series of Gaussian functions[62,63] to better capture how the intensities of any unresolved conformations change over time. We model the cross section profile with a fixed set of Gaussian functions, each of which represents a different conformer. The peak heights are varied to find the best fit at each time point, which reveals the changes in conformer abundances over time.

A minimum of four Gaussian functions are required to model the CCS distributions for the doubly charged ion of Phe[1]–Pro[2]–Gly_3–Lys^6. These four Gaussians, centered at $^{DT}CCS_{He}$ values of 156, 158, 160, and 163 Å[2], are shown in Figure 4 (left). The abundances of the conformations of reactant and product ions at different times are plotted in Figure 4 (right). The Phe[1]–Pro[2]–Gly_3–Lys^6 doubly charged

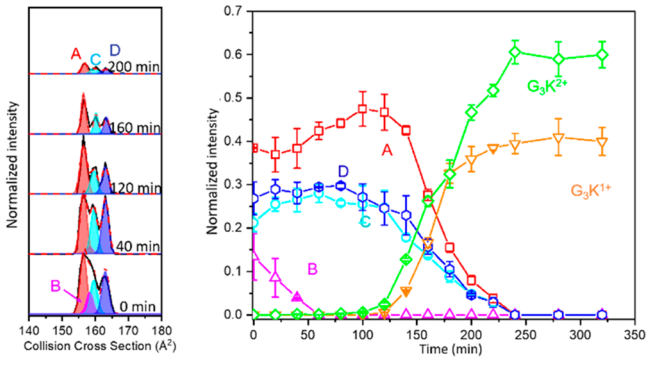

Figure 4. (left) Collison cross section distribution for $[FPG_3K + 2H]^{2+}$ at different incubation times in ethanol with 1% acetic acid (by volume) under 75 °C. Gaussian functions representing conformation types that are assigned to A, B, C, and D with the peak center at 156, 158, 160, and 163 Å[2], respectively. The sum of Gaussian functions is drawn as red dashed lines. The experimental data are plotted as black solid lines. (right) Kinetics data of peptide Phe[1]–Pro[2]–Gly_3–Lys^6 dissociation in ethanol with 1% acetic acid (by volume).

https://doi.org/10.1021/acs.jpcb.1c03515
J. Phys. Chem. B 2021, 125, 8107–8116

ion distribution initially contains ~39% A, ~13% B, ~21% C, and ~27% D. Prior to dissociation, the intensities of these three conformations vary as time progresses: an obvious increase in conformer A has been found. C and D maintain relatively the same abundance before dissociation. Conformer B decreases in abundance and disappears at 60 min. Combining the Gaussian fitting and alanine substitution results, we believe that conformations A, C, and D contain a *cis* penultimate proline while B contains a *trans* penultimate proline. Conformation A is grouped as *cis* because its abundance increases during the induction period, which is likely due to the increase in *cis* isomer from *trans* → *cis* isomerization. During the incubation, *trans*-Phe^1−Pro^2−Gly$_3$−Lys^6 (B) absorbs energy and undergoes *trans* → *cis* isomerization of the Phe^1−Pro^2 peptide bond, resulting in an increase in abundance of *cis*-Phe^1−Pro^2−Gly$_3$−Lys^6 (A). At around 120 min, the *cis*-conformer start to dissociate, and the dissociation process completes at around 240 min.

The doubly charged precursor ions of Phe^1−Pro^2−Gly$_n$−Lys^{n+3} (n = 1, 2, 4, 5, 6, and 7) present a single peak in CCS distribution profiles during the dissociation process. Figure 5

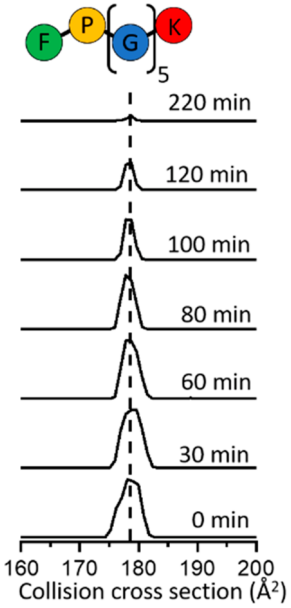

Figure 5. CCS of doubly charged peptide Phe^1−Pro^2−Gly$_5$−Lys^8 at different incubation times. The full width half-maximum is decreased during the dissociation.

shows the CCS distribution of $[FPG_5K + 2H]^{2+}$ at different incubation times. The peak center stays at relatively the same position, but there is an obvious decrease in full width at half-maximum (fwhm) before dissociation occurs. CCS distributions of peptides containing 1, 2, 4, 5, 6, and 7 glycine residues show a similar decrease in fwhm and are shown in Supporting Information Figure S3. This suggests that, similar to Phe^1−Pro^2−Gly$_3$−Lys^6, the number of conformers is decreasing with time as the *trans* → *cis* isomerization of the Phe^1−Pro^2 bond occurs during the incubation. However, unlike the change in the mobility distribution of $[FPG_3K + 2H]^{2+}$ during the dissociation, we are unable to identify multiple conformers by fitting with Gaussian functions. Therefore, it is likely that these peptides contain both *cis*- and *trans*-isomers that have close CCS values, making it hard to resolve in IMS dimension.

For Phe^1−Pro^2−Gly$_8$−Lys^{11}, the ratio between *cis*- and *trans*-isomers changes as the dissociation progresses, which is discussed in detail in a previous study.[35]

Insight into Peptide Structures and Stabilities in Solution through MD Simulations. In order to further understand the length effect on the rate of DKP formation, MD simulations were performed on peptide Phe^1−Pro^2−Gly$_n$−Lys^{n+3} (n = 1, 2, and 9). Figure 6 shows five

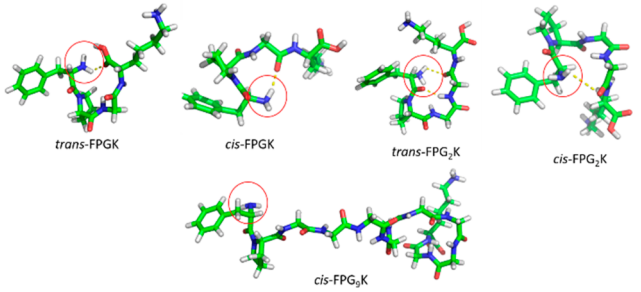

Figure 6. Representative low energy structures of $[FPGK + H]^+$, $[FPG_2K + H]^+$, and $[FPG_9K + H]^+$ obtained from MD simulations (the simulations start with both *trans*- and *cis*-helical structures for n = 1 and n = 2 peptides and *cis*-helical structures for n = 9 peptide). Amino acid chains are labeled for clarity. H-Bonds are represented as yellow dashed lines. The amino group involved in the DKP formation is circled.

representative low-energy structures for these peptide ions following 1 ns of dynamics in explicit solvent. In $[FPGK + H]^+$ and $[FPG_2K + H]^+$ structures, a hydrogen bond formed between the amino group of Phe^1 and either the carboxylic group or carbonyl group of the Gly, while there is no such interaction in $[FPG_9K + H]^+$. Glycine is by nature very flexible. In longer peptides, there are additional glycines that result in more extended structures compared to shorter peptides. The intramolecular interaction in short peptides stabilizes the overall structure in solution, thus inhibiting either *trans* → *cis* isomerization of the Phe^1−Pro^2 bond or cleavage of the Pro^2−Gly^3 peptide bond, leading to the DKP formation. In addition, the amino group on the N-terminus is shielded by the hydrogen bonding interaction, disfavoring the nucleophilic attack to the carbonyl group between the second and third residues. Of particular interest is that, in the $[$*trans*-$FPG_2K + H]^+$ structure, one more hydrogen bond formed (between the carbonyl group of Phe^1 and the amino group of Gly^4) compared to $[FPGK + H]^+$ and $[$*cis*-$FPG_2K + H]^+$. This likely explains why peptide FPG_2K is more stable than FPGK and may also lead to a higher fraction of *trans*-isomer in Phe^1−Pro^2−Gly$_2$−Lys^5. It is worth mentioning that, in the MD simulation, the protons are fixed at certain residues; in reality, the protonation sites likely vary over time. This leads us to offer another possible prospect to understand the stability of these peptides. In short peptides, there are fewer stable protonation sites compared to the longer peptides, which makes it more likely that the N-terminus amino group will be charged. Protonation of the N-terminal amino group prevents the nucleophilic attack on the nearby carbonyl group, which is a key step in DKP formation, thus increasing the stability of the short peptides compared to longer ones.

Exploring Dissociation Pathways for Peptide Phe^1−Pro^2−Gly$_n$−Lys^{n+3}. A number of potential pathways are modeled and compared in order to understand the mechanism behind the dissociation processes. More details of this

https://doi.org/10.1021/acs.jpcb.1c03515
J. Phys. Chem. B 2021, 125, 8107−8116

approach can be found in previous studies.[27,64] For Phe^1–Pro^2–Gly_n–Lys^{n+3} (n = 1, 2, 4, 5, and 7), although there may be *cis*-isomers in the initial distributions, the *trans* → *cis* isomerization of the Phe^1–Pro^2 peptide bond must occur prior to dissociation, as the *cis*-isomer is the only conformer that undergoes DKP formation. Determination of the dissociation mechanism of peptide Phe^1–Pro^2–Gly_5–Lys^8 is shown here as an example of the process. At first, we fit the experimental data with the simplest one-step mechanism—a direct transition between the initial peptide Phe^1–Pro^2–Gly_5–Lys^8 and its dissociation product peptide fragment Gly_5–Lys^6 with no intermediate structures in between, as shown by the following reaction:

$$[FPG_5K + 2H]^{2+} \rightarrow [G_5K + 2H]^{2+} + cFP \quad (2)$$

This model is shown in Table S1 as model 1. In Figure 7, the dashed lines represent the best fit of this model for the kinetics

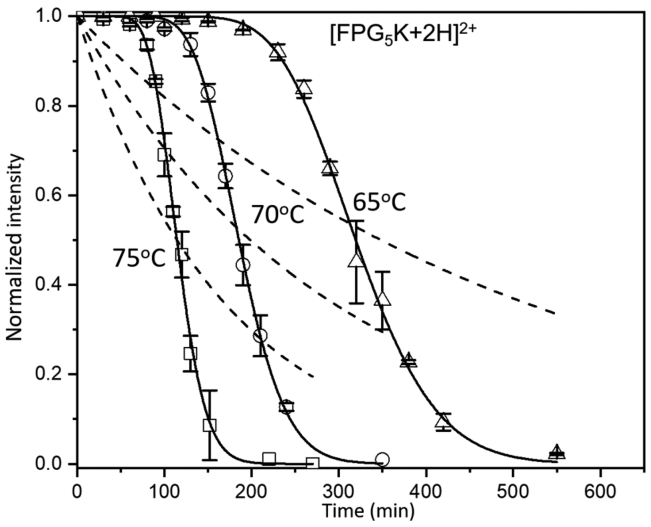

Figure 7. Peptide Phe^1–Pro^2–Gly_5–Lys^8 dissociation kinetics plots in ethanol at 75 °C (hollow rectangles), 70 °C (circles), and 65 °C (circles) with 1% acetic acid (by volume). The sequential unimolecular kinetics model is employed to fit the data. The dashed lines represent the simplest fitting model 1, as shown in Table S1. The solid lines represent the best-fitting model under different temperatures. The number of unseen intermediates involved in the dissociation pathway that produces the minimum residue sum of squares value considering the three temperatures is 19. The dissociation half-lives are 115, 187, and 322 min under 75, 70, and 65 °C, respectively.

data. The curves miss most of the data points, and therefore, this mechanism is a poor model. Sixteen other candidate pathways are also listed and compared in Table S1: the best-fitting model among all of these is model 13 with the lowest fitting residuals. This model is a sequential unimolecular mechanism with 19 unseen intermediates and the same rate constant associated with each transition among multiple intermediate states. These intermediates are referred to as unseen intermediates because they are not detected by IMS-MS but are derived from the best-fitting model as described previously.[64] This fit is shown as solid curves in Figure 7. Based on this approach, we generate best-fitting curves for other peptides in this family. Kinetic data and the best-fitting curves for Phe^1–Pro^2–Gly_n–Lys^{n+3} (n = 1, 2, 4, 5, 6, 7, and 9) appear in Figures S4–S9 in the Supporting Information (analogous figures for peptide Phe^1–Pro^2–Gly_8–Lys^{11} are shown in a previous study[35]). The mechanism and the corresponding sum of squares of the fitting residuals (ΣRSS) are listed in Tables S2–S7. For Phe^1–Pro^2–Gly_n–Lys^{n+3} (n = 1, 2, 4, 5, and 7), since the initial peptide contains *trans*-isomer, the derived number of intermediates is the total number involved in both the *trans* → *cis* isomerization of the Phe^1–Pro^2 peptide bond and the *cis*-isomer dissociation steps. Since Phe^1–Pro^2–Gly_9–Lys^{12} contains only the *cis*-isomer, the intermediates in this case are all for the *cis*-isomer dissociation step.

In the dissociation processes for peptides containing 1, 2, 4, 5, 6, and 7 glycine linkers, 25, 25, 17, 19, 7, and 4 intermediates are involved, respectively. For Phe^1–Pro^2–Gly_8–Lys^{11}, two and three intermediates are involved in *trans* → *cis* isomerization of the Phe^1–Pro^2 peptide bond and the *cis*-isomer dissociation, respectively, as described in a previous paper.[35] For Phe^1–Pro^2–Gly_9–Lys^{12}, one intermediate is involved in the *cis*-conformer dissociation step.

For peptide Phe^1–Pro^2–Gly_3–Lys^6, conformers C and D show a similar dissociation pattern, while conformer B converts to A before dissociation. After the abundance curves of A and the singly charged product ion $[G_3K + H]^+$ intersect, the continuing decrease in A is nearly mirrored by the increase in the product ion. This correlation suggests that A converts to $[G_3K + H]^+$ while C and D convert to $[G_3K + 2H]^{2+}$ during the dissociation process. Conformers A, B, and $[G_3K + H]^+$ are fitted as a group, while conformers C, D, and $[G_3K + H]^{2+}$ are fitted as another group. After comparing a number of mechanisms (Supporting Information, Tables S8 and S9), the best-fitting model is shown as follows:

$$B \rightarrow i_1 \rightarrow i_2 \rightarrow A \rightarrow i_1 \rightarrow \ldots \rightarrow i_{16} \rightarrow G_3K^{2+} \quad (3)$$

$$C \rightarrow i_1 \rightarrow \ldots \rightarrow i_{18} \rightarrow G_3K^{2+} \quad (4)$$

$$D \rightarrow i_1 \rightarrow \ldots \rightarrow i_{18} \rightarrow G_3K^{2+} \quad (5)$$

The best-fitting curves are shown in the Supporting Information (Figures S10–S12). A total of 18 intermediates are necessary in order to model the dissociation curves of C and D. Considering the similar dissociation curves of C and D, it is possible that C and D come from the same solution conformer. A total of 16 intermediates are needed to fit with the degradation of conformer A. The transition of conformer B to conformer A (*trans* → *cis* isomerization of the Phe^1–Pro^2 peptide bond) involves two intermediates, the number of which is equal to the *trans* → *cis* isomerization process of Phe^1–Pro^2–Gly_8–Lys^{11} in ethanol.[35] The difference in stability of Phe^1–Pro^2–Gly_3–Lys^6 compared to Phe^1–Pro^2–Gly_8–Lys^{11} can be largely attributed to the different number of intermediates involved in the *cis*-isomer dissociation process.

In general, fewer intermediates are derived for dissociation of longer peptides. This may be due to the idea that a longer, more flexible glycine chain poses fewer restrictions on the processes that lead to dissociation at the N-terminus. This allows for less steps to reach to dissociation intermediate.

Calculation of Transition State Thermodynamic Values. We use the rate constants obtained by fitting data from different temperatures to construct Arrhenius plots for these peptides according to eq 6:

$$\ln(k) = \frac{-E_a}{R}\frac{1}{T} + \ln(A) \quad (6)$$

https://doi.org/10.1021/acs.jpcb.1c03515
J. Phys. Chem. B 2021, 125, 8107–8116

Table 2. Summary of Transition State Thermodynamic Data of Peptide $Phe^1-Pro^2-Gly_n-Lys^{n+3}$ (n = 1−9)

n	m[c]	$\Delta G^{\ddagger}$ (kJ·mol^{-1})	$\Delta H^{\ddagger}$ (kJ·mol^{-1})	$\Delta S^{\ddagger}$ (J·mol^{-1}·K^{-1})	E_a (kJ·mol^{-1})
1	25	100.3 ± 1.5	113.4 ± 1.1	44.0 ± 3.2	110.9 ± 1.1
2	25	101.5 ± 1.9	116.7 ± 1.5	50.8 ± 4.2	114.2 ± 1.5
3[a]	16	98.5 ± 4.5	106.7 ± 4.5	27.3 ± 0.6	102.2 ± 7.7
3[b]	2	97.7 ± 2.6	104.7 ± 2.5	23.4 ± 2.9	102.2 ± 2.5
3[c]	18	98.3 ± 1.0	108.5 ± 0.8	34.1 ± 2.0	106.0 ± 0.8
3[d]	18	98.7 ± 4.8	108.6 ± 4.6	33.1 ± 5.0	106.1 ± 4.6
4	17	94.6 ± 0.9	93.2 ± 0.7	−4.7 ± 2.0	90.7 ± 0.7
5	19	96.7 ± 0.9	102.9 ± 0.7	20.8 ± 2.1	100.5 ± 0.7
6	7	96.7 ± 1.2	89.1 ± 0.9	−25.4 ± 2.6	86.6 ± 0.9
7	4	101.5 ± 0.5	112.1 ± 0.4	35.7 ± 1.1	109.6 ± 0.4
8[f]	2	100.5 ± 1.1	106.0 ± 0.5	18.4 ± 3.4	103.5 ± 0.5
8[g]	3	99.9 ± 3.7	109.5 ± 3.4	31.9 ± 5.5	107.0 ± 3.4
9	1	98.1 ± 0.2	102.9 ± 0.1	16.0 ± 0.6	100.4 ± 0.1

[a]Conformer A of $Phe^1-Pro^2-Gly_3-Lys^6$. [b]Conformer B of $Phe^1-Pro^2-Gly_3-Lys^6$. [c]Conformer C of $Phe^1-Pro^2-Gly_3-Lys^6$. [d]Conformer D of $Phe^1-Pro^2-Gly_3-Lys^6$. [e]m represents the number of unseen intermediates derived from the best-fitting model. [f]*trans* → *cis* isomerization process. [g]*cis*-conformer dissociation process.

(Supporting Information, Figures S13−S23). The pre-exponential factor (A) and activation energy (E_a) are derived from the y-intercept and slope of the best-fitting line. Equations 7 and 8 were then used to parse the contributions of enthalpy and entropy at the transition state

$$\Delta H^{\ddagger} = E_a + RT \tag{7}$$

$$\Delta S^{\ddagger} = R \ln \frac{Ah}{eTk_b} \tag{8}$$

$$\Delta G^{\ddagger} = \Delta H^{\ddagger} - T\Delta S^{\ddagger} \tag{9}$$

where h is Planck's constant, k_B is Boltzmann's constant, R is the gas constant, T is the temperature of the reaction, and e is Euler's number. Gibbs free energies for each transition state ($\Delta G^{\ddagger}$) are calculated from $\Delta H^{\ddagger}$ and $\Delta S^{\ddagger}$ according to eq 9.

The derived transition state thermodynamic values as well as the number of intermediates involved in the dissociation process are listed in Table 2. The transition states leading to dissociation of the peptides in this family are enthalpically disfavored. The n = 4 and n = 6 peptides have entropic barriers ($\Delta S^{\ddagger} < 0$), while transition states of all of the other peptides are entropically favored ($\Delta S^{\ddagger} > 0$). This suggests that the initial structures of n = 4 and n = 6 peptides are more entropically favored compared to other peptides in this family. Therefore, we can divide peptides in this family into two groups—(1) n = 4 and 6 peptides and (2) other peptides—and study the thermodynamics for the dissociation.

In general, the dissociation half-life is correlated with two factors: (1) the number of transition states is positively correlated to the length of the induction period; (2) a lower transition state Gibbs free energy barrier leads to a more rapid dissociation. For peptides with one and two glycine linkers, the Gibbs free energy barriers are 100.3 ± 1.5 and 101.5 ± 1.9 kJ·mol^{-1}, respectively. This aligns with these peptides' kinetic stability. Although they proceed through the same number of intermediates, the energetic barriers for these peptides differ, with the more stable peptide having the higher energy barrier during dissociation. This is reasonable because a higher proportion of intramolecular hydrogen bonding in the n = 2 peptide compared to the n = 1 peptide leads to a greater initial ordering effect in the n = 2 peptide, as shown by our MD simulations. In addition, the intramolecular hydrogen bonds break as these peptides rearrange their structures and undergo *trans* → *cis* isomerization of the Phe^1-Pro^2 peptide bond. New hydrogen bonding interactions between peptide and solvent are formed. Breaking the intramolecular interactions frees more groups in the n = 2 peptide compared to the n = 1 peptide, which will form intermolecular hydrogen bonding interactions with solvent molecules and provide an additional disordering effect for the n = 2 peptide compared to the n = 1 peptide. This enthalpy−entropy compensation effect is also shown in a previous dissociation study.[35]

All of the conformers in the n = 3 peptide have a smaller number of transition states compared to the n = 1 and 2 peptides. In addition, the transition state Gibbs free energy barrier of the n = 3 peptide is smaller than the n = 1 and 2 peptides. Both of these findings imply a shorter dissociation half-life of n = 3 peptide compared to n = 1 and n = 2 peptides. In n = 3 peptide, conformers C and D have similar dissociation kinetics, and the transition state thermodynamic values for these conformers are similar. It is worth mentioning that the derived Gibbs free energy value for *trans* → *cis* isomerization of the peptide bond is close to the values for the dissociation of conformers A, C, and D. The n = 8 peptide also shows similarity in isomerization and dissociation energy barriers in a previous study.[35]

The n = 5 peptide has more intermediates compared to the n = 7 peptide, but the transition state Gibbs free energy barrier of the n = 5 peptide is smaller than that of the n = 7 peptide. In this case, the higher number of intermediates causes the longer dissociation half-life of the n = 5 peptide.

The n = 9 peptide contains only *cis*-isomer; therefore, the transition state thermodynamic values we calculated here are for dissociation of the *cis*-isomer. Compared to our previously reported n = 8 peptide *cis*-isomer dissociation process, fewer intermediate states are involved in the n = 9 peptide. In addition, the dissociation process of the n = 9 peptide has a lower enthalpic barrier and is slightly less entropically favored compared to n = 8 peptide dissociation. These findings align with the faster dissociation rate of n = 9 peptide compared to n = 8 peptide.

In the case of n = 4 and 6 peptides, the dissociation process for n = 4 peptide involves a large number of intermediates with low barriers, while n = 6 shows a higher barrier with a small number of intermediates. The shorter half-life for n = 4 implies

https://doi.org/10.1021/acs.jpcb.1c03515
J. Phys. Chem. B 2021, 125, 8107−8116

that the relative stability of these two peptides correlates more strongly to the Gibbs free energy of activation than to the number of intermediates.

Most of these peptides' dissociation half-lives are controlled by the number of intermediates involved in the dissociation. For a few peptides, the half-lives are dependent on the transition state Gibbs free energy barriers. This may be because, for n = 1, 2, 4, 5, 6, and 7 peptides, there is only a mobility peak that aligns with the *trans*-penultimate proline, but there may be a *cis*-conformer within that mobility distribution that cannot be separated with our IMS resolving power.

CONCLUSIONS

This work aimed to investigate the dissociation kinetics of Phe^1–Pro^2–Gly_n–Lys^{n+3} (n = 1–9). By comparing the dissociation half-lives, we obtained the stability information for these peptides. Substitution of alanine for proline demonstrated that the initial mixture for most Phe^1–Pro^2–Gly_n–Lys^{n+3} contains *trans*-Pro^2, though Phe^1–Pro^2–Gly_9–Lys^{12} appears to have exclusively *cis*-Pro^2. By applying Gaussian function fitting to the dissociation process of Phe^1–Pro^2–Gly_3–Lys^6, we successfully identified different conformers and tracked the abundance change of each *cis*- and *trans*-isomer with time. MD simulations were conducted in order to understand the stabilities of peptides with different lengths. From these experimental and theoretical results, we learned the following: (1) most of the shorter peptides have longer dissociation half-lives compared to longer peptides; (2) in general, longer induction periods and more intermediates are involved in the dissociation of shorter peptides than in longer ones; (3) MD simulations suggest that the short peptides tend to adopt folded structures stabilized by intramolecular hydrogen bonding which inhibits DKP formation, while long peptides prefer extended structures in solution. The change in the number of intermediates that yields the best fit as peptide length changes suggests that the critical change that leads to structure preference likely occurs at six glycines. In addition, there are fewer protonation sites in shorter peptides compared to longer peptides. Therefore, the chance of the N-terminus amino group being charged is larger in shorter peptides, which will inhibit the nucleophilic attack involved in the DKP formation reaction. Sequential unimolecular models are used to fit with the induction period prior to dissociation. Transition state thermodynamic values for these peptides are derived from self-cleavage experiments at different temperatures. The transition state Gibbs free energy values for these peptides are in a close range, which indicates there is an enthalpy–entropy compensation similar to findings in a previous study.[35] The dissociation process is enthalpically disfavored and slightly entropically favored; this process is primarily controlled by transition state enthalpy. The relationship between peptide length and stability as well as the transition state thermodynamic features derived from this paper could serve as a guide for designing stable cancer vaccines. If a peptide vaccine with penultimate proline requires a longer sequence in order to generate the desired immune response, then testing for stability is warranted.

ASSOCIATED CONTENT

Supporting Information

The Supporting Information is available free of charge at https://pubs.acs.org/doi/10.1021/acs.jpcb.1c03515.

Schematic diagram of the 2 m IMS–IMS–MS instrument (Figure S1); collison cross section distribution for peptide FPG_nK (n = 1, 2, 4, 6, and 7) and their Pro^2 to Ala substituted peptide (Figure S2); collison cross section distribution for peptide FPG_nK (n = 1, 2, 4, 6–9) at different incubation times (Figure S3); dissociation kinetics plots of peptide FPG_nK (n = 1–7 and 9) (Figures S4–S14); Arrhenius plot for peptide FPG_nK (n = 1–7 and 9) (Figures S13–S23); and residual sums of squares values for peptide FPG_nK (n = 1–7 and 9) dissociation (Figures S24–S32) (PDF)

AUTHOR INFORMATION

Corresponding Authors

David A. Hales – *Department of Chemistry, Hendrix College, Conway, Arkansas, United States*; Email: hales@hendrix.edu

David E. Clemmer – *Department of Chemistry, Indiana University, Bloomington, Indiana, United States*; orcid.org/0000-0003-4039-1360; Email: clemmer@indiana.edu

Authors

Zhichao Zhang – *Department of Chemistry, Indiana University, Bloomington, Indiana, United States*

Christopher R. Conant – *Department of Chemistry, Indiana University, Bloomington, Indiana, United States;* Present Address: Pacific Northwest National Laboratory, Portland, OR, United States

Tarick J. El-Baba – *Department of Chemistry, Indiana University, Bloomington, Indiana, United States;* Present Address: University of Oxford, Oxfordshire, United Kingdom.

Shannon A. Raab – *Department of Chemistry, Indiana University, Bloomington, Indiana, United States;* Present Address: Eli Lilly and Company, Indianapolis, IN, United States.

Daniel R. Fuller – *Department of Chemistry, Indiana University, Bloomington, Indiana, United States;* Present Address: Novartis Institutes for BioMedical Research, Boston, MA, United States.

Complete contact information is available at: https://pubs.acs.org/10.1021/acs.jpcb.1c03515

Notes

The authors declare no competing financial interest.

ACKNOWLEDGMENTS

This work is supported in part by funds from the National Institutes of Health grants 5R01GM121751-0 (D.E.C.), the Robert and Marjorie Mann Graduate Research Fellowship (Z.Z., C.R.C., S.A.R., D.R.F.) from Indiana University, the Dissertation Research Award from the Indiana University College of Arts and Sciences (T.J.E.-B.), and a Faculty Project Grant from Hendrix College (D.A.H.). We thank Fa Zhang in the Dimarchi lab for help with peptide synthesis.

REFERENCES

(1) Epstein, C. J.; Goldberger, R. F.; Anfinsen, C. B. The genetic control of tertiary protein structure: studies with model systems. *Cold Spring Harbor Symp. Quant. Biol.* **1963**, *28*, 439–449.

(2) Kendrew, J. C.; Bodo, G.; Dintzis, H. M.; Parrish, R.; Wyckoff, H.; Phillips, D. C. A three-dimensional model of the myoglobin molecule obtained by x-ray analysis. *Nature* **1958**, *181*, 662−666.
(3) Matouschek, A.; Kellis, J. T.; Serrano, L.; Fersht, A. R. Mapping the transition state and pathway of protein folding by protein engineering. *Nature* **1989**, *340*, 122−126.
(4) McCammon, J. A.; Gelin, B. R.; Karplus, M. Dynamics of folded proteins. *Nature* **1977**, *267*, 585−590.
(5) Henzler-Wildman, K.; Kern, D. Dynamic personalities of proteins. *Nature* **2007**, *450*, 964−972.
(6) Jarvet, J.; Damberg, P.; Bodell, K.; Göran Eriksson, L.; Graeslund, A. Reversible random coil to β-sheet transition and the early stage of aggregation of the Aβ (12- 28) fragment from the Alzheimer peptide. *J. Am. Chem. Soc.* **2000**, *122*, 4261−4268.
(7) Manning, M. C.; Chou, D. K.; Murphy, B. M.; Payne, R. W.; Katayama, D. S. Stability of protein pharmaceuticals: an update. *Pharm. Res.* **2010**, *27*, 544−575.
(8) Werle, M.; Bernkop-Schnürch, A. Strategies to improve plasma half life time of peptide and protein drugs. *Amino Acids* **2006**, *30*, 351−367.
(9) Powell, M. F.; Grey, H.; Gaeta, F.; Sette, A.; Colón, S. Peptide stability in drug development: a comparison of peptide reactivity in different biological media. *J. Pharm. Sci.* **1992**, *81*, 731−735.
(10) Powell, M. F.; Stewart, T.; Urge, L.; Gaeta, F. C.; Sette, A.; Arrhenius, T.; Thomson, D.; Soda, K.; Colon, S. M. Peptide stability in drug development. II. Effect of single amino acid substitution and glycosylation on peptide reactivity in human serum. *Pharm. Res.* **1993**, *10*, 1268−1273.
(11) Patel, K.; Borchardt, R. T. Chemical pathways of peptide degradation. II. Kinetics of deamidation of an asparaginyl residue in a model hexapeptide. *Pharm. Res.* **1990**, *7*, 703−711.
(12) Geiger, T.; Clarke, S. Deamidation, isomerization, and racemization at asparaginyl and aspartyl residues in peptides. Succinimide-linked reactions that contribute to protein degradation. *J. Biol. Chem.* **1987**, *262*, 785−794.
(13) Li, S.; Schöneich, C.; Wilson, G. S.; Borchardt, R. T. Chemical pathways of peptide degradation. V. Ascorbic acid promotes rather than inhibits the oxidation of methionine to methionine sulfoxide in small model peptides. *Pharm. Res.* **1993**, *10*, 1572−1579.
(14) Collins, M.; Waite, E.; Van Duin, A. Predicting protein decomposition: the case of aspartic-acid racemization kinetics. *Philos. Trans. R. Soc., B* **1999**, *354*, 51−64.
(15) Goolcharran, C.; Khossravi, M.; Borchardt, R. T. Chemical pathways of peptide and protein degradation; *Pharmaceutical formulation and development of peptides and proteins*; Taylor and Francis: London, 2000; pp 70−88.
(16) Møss, J.; Bundgaard, H. Kinetics and mechanism of the facile cyclization of histidyl-prolineamide to cyclo (His-Pro) in aqueous solution and the competitive influence of human plasma. *J. Pharm. Pharmacol.* **2011**, *42*, 7−12.
(17) Giralt, E.; Eritja, R.; Pedroso, E. Diketopiperazine formation in acetamido-and nitrobenzamido-bridgedpolymeric supports. *Tetrahedron Lett.* **1981**, *22*, 3779−3782.
(18) Mohammed, F.; Cobbold, M.; Zarling, A. L.; Salim, M.; Barrett-Wilt, G. A.; Shabanowitz, J.; Hunt, D. F.; Engelhard, V. H.; Willcox, B. E. Phosphorylation-dependent interaction between antigenic peptides and MHC class I: a molecular basis for the presentation of transformed self. *Nat. Immunol.* **2008**, *9*, 1236−1243.
(19) Cobbold, M.; De La Peña, H.; Norris, A.; Polefrone, J. M.; Qian, J.; English, A. M.; Cummings, K. L.; Penny, S.; Turner, J. E.; Cottine, J. MHC class I-associated phosphopeptides are the targets of memory-like immunity in leukemia. *Sci. Transl. Med.* **2013**, *5*, 203ra125.
(20) Townsend, A.; Bodmer, H. Antigen recognition by class I-restricted T lymphocytes. *Annu. Rev. Immunol.* **1989**, *7*, 601−624.
(21) York, I. A.; Rock, K. L. Antigen processing and presentation by the class I major histocompatibility complex. *Annu. Rev. Immunol.* **1996**, *14*, 369−396.
(22) Cox, A. L.; Skipper, J.; Chen, Y.; Henderson, R. A.; Darrow, T. L.; Shabanowitz, J.; Engelhard, V. H.; Hunt, D. F.; Slingluff, C. L. Identification of a peptide recognized by five melanoma-specific human cytotoxic T cell lines. *Science* **1994**, *264*, 716−719.
(23) Chianese-Bullock, K. A.; Lewis, S. T.; Sherman, N. E.; Shannon, J. D.; Slingluff, C. L., Jr. Multi-peptide vaccines vialed as peptide mixtures can be stable reagents for use in peptide-based immune therapies. *Vaccine* **2009**, *27*, 1764−1770.
(24) Kristensen, D.; Chen, D.; Cummings, R. Vaccine stabilization: research, commercialization, and potential impact. *Vaccine* **2011**, *29*, 7122−7124.
(25) Fuller, D. R.; Conant, C. R.; El-Baba, T. J.; Brown, C. J.; Woodall, D. W.; Russell, D. H.; Clemmer, D. E. Conformationally regulated peptide bond cleavage in bradykinin. *J. Am. Chem. Soc.* **2018**, *140*, 9357−9360.
(26) Fuller, D. R.; Conant, C. R.; El-Baba, T. J.; Zhang, Z.; Molloy, K. R.; Zhang, C. S.; Hales, D. A.; Clemmer, D. E. Monitoring the stabilities of a mixture of peptides by mass-spectrometry-based techniques. *Eur. J. Mass Spectrom.* **2019**, *25*, 73−81.
(27) Conant, C. R.; Fuller, D. R.; El-Baba, T. J.; Zhang, Z.; Russell, D. H.; Clemmer, D. E. Substance P in solution: trans-to-cis configurational changes of penultimate prolines initiate non-enzymatic peptide bond cleavages. *J. Am. Soc. Mass Spectrom.* **2019**, *30*, 919−931.
(28) Clemmer, D. E.; Jarrold, M. F. Ion mobility measurements and their applications to clusters and biomolecules. *J. Mass Spectrom.* **1997**, *32*, 577−592.
(29) Bohrer, B. C.; Merenbloom, S. I.; Koeniger, S. L.; Hilderbrand, A. E.; Clemmer, D. E. Biomolecule analysis by ion mobility spectrometry. *Annu. Rev. Anal. Chem.* **2008**, *1*, 293−327.
(30) Donkin, J. J.; Turner, R. J.; Hassan, I.; Vink, R. Substance P in traumatic brain injury. *Prog. Brain Res.* **2007**, *161*, 97−109.
(31) Hökfelt, T.; Pernow, B.; Wahren, J. Substance P: a pioneer amongst neuropeptides. *J. Intern. Med.* **2001**, *249*, 27−40.
(32) O'Connor, T. M.; O'Connell, J.; O'Brien, D. I.; Goode, T.; Bredin, C. P.; Shanahan, F. The role of substance P in inflammatory disease. *J. Cell. Physiol.* **2004**, *201*, 167−180.
(33) Wang, W. F.; Yang, Y. S.; Peng, L. H.; Sun, G. Alternation of substance P-containing neural pathways in a rat model of irritable bowel syndrome with rectal distension. *Chin. J. Dig. Dis.* **2006**, *7*, 211−218.
(34) Pernow, B. Studies on substance P; purification, occurrence and biological actions. *Acta Physiol. Scand., Suppl.* **1953**, *29*, 1−89.
(35) Zhang, Z.-c.; Raab, S. A.; Hales, D. A.; Clemmer, D. E. Influence of Solvents upon Diketopiperazine Formation of FPG_8K. *J. Phys. Chem. B* **2021**, *125*, 2952−2959.
(36) Frackenpohl, J.; Arvidsson, P. I.; Schreiber, J. V.; Seebach, D. The outstanding biological stability of β-and γ-peptides toward proteolytic enzymes: an in vitro investigation with fifteen peptidases. *ChemBioChem* **2001**, *2*, 445−455.
(37) Capasso, S.; Mazzarella, L. Solvent effects on diketopiperazine formation from N-terminal peptide residues. *J. Chem. Soc., Perkin Trans. 2* **1999**, 329−332.
(38) Goolcharran, C.; Borchardt, R. T. Kinetics of diketopiperazine formation using model peptides. *J. Pharm. Sci.* **1998**, *87*, 283−288.
(39) Purdie, J. E.; Benoiton, N. L. Piperazinedione formation from esters of dipeptides containing glycine, alanine, and sarcosine: the kinetics in aqueous solution. *J. Chem. Soc., Perkin Trans. 2* **1973**, 1845−1852.
(40) Steinberg, S. M.; Bada, J. L. Peptide decomposition in the neutral pH region via the formation of diketopiperazines. *J. Org. Chem.* **1983**, *48*, 2295−2298.
(41) El-Baba, T. J.; Fuller, D. R.; Hales, D. A.; Russell, D. H.; Clemmer, D. E. Solvent mediation of peptide conformations: polyproline structures in water, methanol, ethanol, and 1-propanol as determined by ion mobility spectrometry-mass spectrometry. *J. Am. Soc. Mass Spectrom.* **2019**, *30*, 77−84.
(42) Pierson, N. A.; Chen, L.; Valentine, S. J.; Russell, D. H.; Clemmer, D. E. Number of solution states of bradykinin from ion

https://doi.org/10.1021/acs.jpcb.1c03515
J. Phys. Chem. B 2021, 125, 8107−8116

mobility and mass spectrometry measurements. *J. Am. Chem. Soc.* **2011**, *133*, 13810−13813.
(43) Shi, L.; Holliday, A. E.; Shi, H.; Zhu, F.; Ewing, M. A.; Russell, D. H.; Clemmer, D. E. Characterizing intermediates along the transition from polyproline I to polyproline II using ion mobility spectrometry-mass spectrometry. *J. Am. Chem. Soc.* **2014**, *136*, 12702−12711.
(44) Coin, I.; Beyermann, M.; Bienert, M. Solid-phase peptide synthesis: from standard procedures to the synthesis of difficult sequences. *Nat. Protoc.* **2007**, *2*, 3247.
(45) Shi, L.; Holliday, A. E.; Glover, M. S.; Ewing, M. A.; Russell, D. H.; Clemmer, D. E. Ion mobility-mass spectrometry reveals the energetics of intermediates that guide polyproline folding. *J. Am. Soc. Mass Spectrom.* **2016**, *27*, 22−30.
(46) Koeniger, S. L.; Merenbloom, S. I.; Sevugarajan, S.; Clemmer, D. E. Transfer of structural elements from compact to extended states in unsolvated ubiquitin. *J. Am. Chem. Soc.* **2006**, *128*, 11713−11719.
(47) Mesleh, M.; Hunter, J.; Shvartsburg, A.; Schatz, G. C.; Jarrold, M. Structural information from ion mobility measurements: effects of the long-range potential. *J. Phys. Chem.* **1996**, *100*, 16082−16086.
(48) Mason, E. A.; McDaniel, E. W. *Transport Properties of Ions in Gases*; John Wiley & Sons: Hoboken, NJ, 1988.
(49) Revercomb, H.; Mason, E. A. Theory of plasma chromatography/gaseous electrophoresis. Review. *Anal. Chem.* **1975**, *47*, 970−983.
(50) Wyttenbach, T.; von Helden, G.; Batka, J. J.; Carlat, D.; Bowers, M. T. Effect of the long-range potential on ion mobility measurements. *J. Am. Soc. Mass Spectrom.* **1997**, *8*, 275−282.
(51) McLean, J. A.; Ruotolo, B. T.; Gillig, K. J.; Russell, D. H. Ion mobility-mass spectrometry: a new paradigm for proteomics. *Int. J. Mass Spectrom.* **2005**, *240*, 301−315.
(52) Kanu, A. B.; Dwivedi, P.; Tam, M.; Matz, L.; Hill, H. H. Ion mobility-mass spectrometry. *J. Mass Spectrom.* **2008**, *43*, 1−22.
(53) Merenbloom, S. I.; Koeniger, S. L.; Valentine, S. J.; Plasencia, M. D.; Clemmer, D. E. IMS- IMS and IMS- IMS- IMS/MS for separating peptide and protein fragment ions. *Anal. Chem.* **2006**, *78*, 2802−2809.
(54) Brazin, K. N.; Mallis, R. J.; Fulton, D. B.; Andreotti, A. H. Regulation of the tyrosine kinase Itk by the peptidyl-prolyl isomerase cyclophilin A. *Proc. Natl. Acad. Sci. U. S. A.* **2002**, *99*, 1899−1904.
(55) Hoaglund, C. S.; Valentine, S. J.; Sporleder, C. R.; Reilly, J. P.; Clemmer, D. E. Three-dimensional ion mobility/TOFMS analysis of electrosprayed biomolecules. *Anal. Chem.* **1998**, *70*, 2236−2242.
(56) Abraham, M. J.; Murtola, T.; Schulz, R.; Páll, S.; Smith, J. C.; Hess, B.; Lindahl, E. GROMACS: High performance molecular simulations through multi-level parallelism from laptops to supercomputers. *SoftwareX* **2015**, *1*, 19−25.
(57) *PyMOL Molecular Graphics System*, version 1.2r3pre; Schrödinger, LLC; https://sourceforge.net/projects/pymol/files/pymol/1.6/ (accessed August 23, 2020).
(58) Kaminski, G. A.; Friesner, R. A.; Tirado-Rives, J.; Jorgensen, W. L. Evaluation and reparametrization of the OPLS-AA force field for proteins via comparison with accurate quantum chemical calculations on peptides. *J. Phys. Chem. B* **2001**, *105*, 6474−6487.
(59) Berendsen, H.; Grigera, J.; Straatsma, T. The missing term in effective pair potentials. *J. Phys. Chem.* **1987**, *91*, 6269−6271.
(60) Darden, T.; York, D.; Pedersen, L. Particle mesh Ewald: An *N*·log (*N*) method for Ewald sums in large systems. *J. Chem. Phys.* **1993**, *98*, 10089−10092.
(61) Glover, M. S.; Dilger, J. M.; Acton, M. D.; Arnold, R. J.; Radivojac, P.; Clemmer, D. E. Examining the influence of phosphorylation on peptide ion structure by ion mobility spectrometry-mass spectrometry. *J. Am. Soc. Mass Spectrom.* **2016**, *27*, 786−794.
(62) Shi, H.; Pierson, N. A.; Valentine, S. J.; Clemmer, D. E. Conformation types of ubiquitin $[M + 8H]^{8+}$ ions from water: methanol solutions: evidence for the N and A states in aqueous solution. *J. Phys. Chem. B* **2012**, *116*, 3344−3352.
(63) Raab, S. A.; El-Baba, T. J.; Woodall, D. W.; Liu, W.; Liu, Y.; Baird, Z.; Hales, D. A.; Laganowsky, A.; Russell, D. H.; Clemmer, D. E. Evidence for Many Unique Solution Structures for Chymotrypsin Inhibitor 2: A Thermodynamic Perspective Derived from vT-ESI-IMS-MS Measurements. *J. Am. Chem. Soc.* **2020**, *142*, 17372−17383.
(64) El-Baba, T. J.; Kim, D.; Rogers, D. B.; Khan, F. A.; Hales, D. A.; Russell, D. H.; Clemmer, D. E. Long-lived intermediates in a cooperative two-state folding transition. *J. Phys. Chem. B* **2016**, *120*, 12040−12046.

https://doi.org/10.1021/acs.jpcb.1c03515
J. Phys. Chem. B 2021, 125, 8107−8116